

DRAFT VERSION FEBRUARY 18, 2022

Preprint typeset using L^AT_EX style AASTeX6 v. 1.0

DEBRIS DISKS AMONG *KEPLER* SOLAR ROTATIONAL ANALOG STARS

R. SILVA SOBRINHO¹, A. D. DA COSTA^{1,2}, B. L. CANTO MARTINS^{1,3}, I. C. LEÃO¹, D. FREIRE DA SILVA¹, M. A. TEIXEIRA¹, M. GOMES DE SOUZA¹, D. B. DE FREITAS⁶, J. P. BRAVO^{1,4}, M. L. DAS CHAGAS⁵, AND J. R. DE MEDEIROS¹

¹Departamento de Física Teórica e Experimental, Universidade Federal do Rio Grande do Norte, Natal, RN
59072-970, Brazil.

²Universidade da Integração da Lusofonia Afro-Brasileira, Redenção, CE 62790-000, Brazil.

³Observatoire de Genève, Université de Genève, Chemin des Maillettes, 51, Sauverny CH - 1290, Switzerland.

⁴Instituto Federal de Educação, Ciência e Tecnologia do Rio Grande do Norte, Natal, RN 59015-000, Brazil.

⁵Faculdade de Física – Instituto de Ciências Exatas, Universidade Federal do Sul e Sudeste do Pará, Marabá, PA
68505-080, Brazil.

and

⁶Departamento de Física, Universidade Federal do Ceará, Campus do Pici, Fortaleza, CE 60455-900, Brazil.

ABSTRACT

Observations of circumstellar disks provide a powerful tool for our understanding of planetary systems dynamics. Analogs to the Solar System asteroid belts, debris disks result from the collision of the remaining solid material of the planet formation process. Even if the presence of disk is now reported for hundreds of stars, its detection around stars similar to the Sun is still very sparse. We report the results of a search for debris disks around *Kepler* stars with surface physical parameters close to solar values, including rotation period, using observations by the Wide-field infrared Survey Explorer (*WISE*). From the entire sample of *Kepler* stars, 881 targets were identified with these parameters and only six of them (KIC 1868785, 7267949, 7435796, 10533222, 11352643, and KIC 11666436) show unambiguous infrared excess, for which we determined debris disk physical parameters. Interestingly, the present study reveals traces of debris disks much more massive and brighter than the Solar System zodiacal dust, probably resulting from recent violent collisional events, orbiting stars with ages around the solar values.

Keywords: infrared: stars – stars: circumstellar matter – stars: solar-type

1. INTRODUCTION

The asteroid belt in our Solar System is located between Mars and Jupiter, i.e., between the inner terrestrial planets and the outer giant planets, with components presenting a large compositional diversity in size and distance from the Sun (DeMeo & Carry 2014). It contains millions of irregularly shaped bodies composed of rocks, ices and metals with a total mass of approximately 4 percent of the Moon or 22 percent of that of Pluto. The presence of water vapor on Ceres, the largest body in the

asteroid belt, and the identification of objects exhibiting apparently cometary activity yet orbiting completely within the main asteroid belt (Hsieh & Jewitt 2006) are the most outstanding recent discoveries related to this region of the Solar System. Observations indicate that at the planetesimal formation stage the location of the snow line, which denotes the radius outside of which ice forms, was within the asteroid belt (e.g., Martin & Livio 2012). Indeed, previous studies claimed that the inner asteroids, closest to Earth, at a radius of about 2.2 AU, were water devoid, whereas the outer asteroids, within a radius around 3.2 AU, were icy objects (Abe et al. 2000). However, more recent studies indicate that asteroids are less segregated by water content than previously believed (DeMeo & Carry 2014).

Although the presence of debris disks, with asteroid belt characteristics, is now well established for hundreds of stars (Chen et al. 2006; Cotten & Song 2016; Trilling et al. 2008; Weissman 1995; Aumann et al. 1984; Patel et al. 2014), the present day literature hints for a scarcity of asteroid belt signatures around Sun-like stars (Da Costa et al. 2017; Sibthorpe et al. 2018). For instance, a recent study has shown a null detection of warm debris around solar twin stars (Da Costa et al. 2017). Given this reality, we report here a search for infrared (IR) excess, a well established diagnostic for circumstellar debris disks, in a sample of 881 *Kepler* main-sequence stars, using observations carried out with the *Wide-field Infrared Survey Explorer* (WISE) (Wright 2010). This space mission mapped the sky at wavelengths 3.4, 4.6, 12, and 22 μm , known as filters W1, W2, W3, and W4, offering a unique laboratory for the search for stellar mid-IR excess. The 12 and 22 μm wavelengths are very sensitive to thermal emissions from objects at temperatures comparable to the Earth, around 300 K, and to the Solar System asteroid belt and interior zodiacal cloud, around 150-250 K.

Indeed, thanks the high quality of the *Kepler* photometric data, we are now able to study a new type of solar analog stars, the solar rotational analogs, namely those stars presenting atmospheric solar parameters and rotation periods similar to the Sun. The stellar sample here analyzed presents these

Table 1. Stellar parameters and fundamental disk properties for the Sun and the stars with confirmed IR excess. Stellar parameters: effective temperature (T_*), surface gravity ($\log g$), metallicity ($[Fe/H]$), were obtained from [Huber et al. \(2014\)](#), rotation periods (P_{rot}) were taken from [McQuillan et al. \(2014\)](#). Disk properties (this work): temperature of the dust (T_d), radius of the debris disk (R_d), dust mass of the disk of circumstellar material (M_d), the fractional luminosity of the dust (f_d).

KIC	T_*	$\log g$	[Fe/H]	P_{rot}	T_d	R_d	M_d	f_d
	(K)	(dex)	(dex)	(days)	(K)	(AU)	($M_\oplus \times 10^{-5}$)	($\times 10^{-4}$)
Sun	5777 ^(a)	4.44 ^(b)	0.00	23.0–33.5 ^(c)	276 ^(d)	< 5.0 ^(d)	$\sim \times 10^{-4}$ ^(d)	$\sim 10^{-3}$ ^(d)
1868785	5837±166	4.50±0.29	-0.16±0.32	24.219±0.232	484 ±22	0.33 ±0.03	2.23 ± 0.57	19.49 ± 3.08
7267949	5629±159	4.42±0.13	-0.42±0.36	25.109±0.457	293 ±13	0.77 ±0.12	5.36 ± 1.98	8.26 ± 1.77
7435796	5902±170	4.43±0.06	0.14±0.18	29.217±0.362	280 ±13	1.07 ±0.12	12.16 ± 4.21	9.60 ± 2.21
10533222	5926±176	4.29±0.16	-0.12±0.26	24.338±0.528	341 ±15	0.82 ±0.15	12.32 ± 4.66	16.63 ± 3.20
11092105	5658±162	4.52±0.04	-0.20±0.28	25.808±0.429	265 ±12	0.90 ±0.09	23.41 ± 7.95	26.41 ± 6.23
11666436	5604±155	4.56±0.03	-0.20±0.30	23.923±0.579	336 ±15	0.52 ±0.05	4.07 ± 1.18	13.48 ± 2.62

References: (a) - [Neckel \(1986\)](#), (b) - [Gray \(1992\)](#), (c) - [Lanza et al. \(2003\)](#), (d) - [Roberge et al. \(2012\)](#)

unique characteristics, surface physical properties similar to the Sun and rotation period ranging P_{rot} from 23 to 33 days. In section 2 of this Letter, we describe the WISE and *Kepler* data used in this study. Section 3 describes the methods used in our analysis of these data. Finally, in Section 4, we present our results and discuss their implications.

2. STELLAR WORKING SAMPLE AND WISE DATA ANALYSIS

2.1. The stellar sample

For the present study, we use a sample of 881 *Kepler* main-sequence stars with surface physical properties close to solar values, that is effective temperature in the range $5579 K < T_{eff} < 5979 K$, superficial gravity in the range $3,94 \text{ cms}^{-2} < \log g < 4,94 \text{ cms}^{-2}$, metallicity $[Fe/H] \sim 0$ and rotation period P_{rot} from 23 to 33 days, namely the range of values of the Sun rotation period. Indeed, we have followed the same strategy by [Das Chagas et al. \(2016\)](#), with rotation period P_{rot} taken from [McQuillan et al. \(2014\)](#).

The *Kepler* coordinates of each target were then used to crosscheck with the 2MASS (Cutri et al. 2003) and full AllWISE (Cutri et al. 2013) catalogs. Assuming a positional accuracy of 5 arcsecond, we find 862 stars with photometry in the three bands of 2MASS (J, H, and K) and in the four WISE bands (W1, W2, W3 and W4). The values of W3 and W4 magnitudes, SNRW3 and SNRW4 signal-to-noise ratios, and the confusion condition flag (ccf), were used as criteria to assess the quality and reliability of WISE data. Checking these photometric properties, we identified 447 stars with fundamental problems such as artifacts contamination (ccf=H,h,P,p,D,d and O,o) (Cutri et al. 2013), high saturation levels ($W3 < 3.8$ or $W4 < -0.4$) and very low signal-to-noise ratio ($SNRW3/W4 < 2.0$). We have therefore disregarded these targets from our sample. Thus, a primary sample of 415 stars with non-saturated photometry, signal-to-noise greater than 2, and unaffected by known artifacts at one or both W3 and W4 bands was analyzed in the search for IR excess only in the band(s) in which no mentioned problem is found.

2.2. Searching for IR excess

Then, the observed spectral energy distribution (SEDs) and model-derived photospheric IR fluxes for each one of the referred 415 stars were compared using the Virtual Observatory Spectral Analyzer (VOSA, Bayo et al. 2008). The SEDs were constructed using the four IR bands W1-W4 from WISE (Cutri et al. 2013), the J, H, and Ks bands from 2MASS (Cutri et al. 2003), and when available, the UBV bands (Mermilliod 2006), the G-band from Gaia (van Leeuwen et al. 2017), and the color bands ugriz from SDSS (Abazajian et al. 2009). For increasing the reliability of IR excess measurements, the theoretical fluxes were computed using three grids of theoretical stellar spectra: Kurucz-ATLAS9 (Castelli et al. 1997), BT-DUSTY (Allard et al. 2012), and BT-NextGen (AGSS2009) (Allard et al. 2012). These models were used to determine the best-fitting line for the observed data by the χ^2 minimization. Only the stars presenting IR excess from the above three models were chosen as

IR excess candidates, amounting to 47 stars (see Table 2 in the online data). We also adopted the estimation of interstellar extinction provided in the *Kepler* database.

For quantification of the observed IR excess, we used the excess significance parameter χ_λ (Beichman et al. 2006; Moór et al. 2006), defined as follows:

$$\chi_\lambda = \frac{F_{\lambda,obs} - F_{\lambda,phot}}{\sqrt{\sigma_{\lambda,obs}^2 + \sigma_{\lambda,cal}^2}}, \quad (1)$$

where $F_{\lambda,obs}$ is the observed flux density and $F_{\lambda,phot}$ is the expected photospheric flux density; $\sigma_{\lambda,obs}$ corresponds to the uncertainties of $F_{\lambda,obs}$; $\sigma_{\lambda,cal}$ refers to the calibration uncertainties of the WISE data of 4.5 % and 5.7 % in the W3 and W4 bands, respectively (Jarrett et al. 2011). Here, we consider as presenting IR excess only those stars for which $\chi_\lambda \geq 2$ (Ribas et al. 2012), corresponding to at least 1.5σ or 87 % significance of deviation from photosphere IR emission ($\chi_\lambda = 0.0$). Based on this criterion, we find a total of 51 stars showing WISE mid-IR excess, although, only 47 stars present such excess in the three theoretical models, as explained before. The difference in significance between the Kurucz and the two other models fluctuates around 10% for the W3 band and 1% for the W4 band. This fluctuation gives us an order of magnitude of the systematic errors associated to the different physical ingredients considered in each model. Our criterion of selecting objects that present excess simultaneously using different models should avoid a bias associated to a particular one (e.g., Sinclair et al. 2010). Statistical errors due to the uncertainty in the fit with the models were not taken into consideration because they are negligible. Maldonado et al. (2017) point out that, for bright objects, the WISE calibration error is dominant in relation to the photometric and theoretical errors. This is not the case for our sample, composed of faint objects, where the photometric error is dominant over to the WISE calibration errors. The values of excess significance and the WISE coordinates for such stars are listed in Table 2 of the online data.

2.3. *WISE image inspection*

In order to identify which stars have a reliable IR excess, with no artificial artifacts or contamination, we applied to the sample of 47 stars the same procedure used by [Da Costa et al. \(2017\)](#) for a visual inspection of the WISE images, based on the identification of some significant problems as PSFs (Point Spread Function) deformed due to an object close to the source, an absent or no evident object, or even caused by nearby objects blended, leading to a misinterpretation of the image. The WISE images were obtained from IRSA (Infrared Science Archive), using $0-3\sigma$ linear scales around $1.7' \times 1.7'$ of each IR excess candidate. In addition, we checked if the IR excess source is a punctual (circular) or elliptical (non-circular) or extensive object, we used a roundness criterion based on ([Cotten & Song 2016](#)), which consists on a comparison of bilateral symmetry of each source determined by a two-dimensional Gaussian adjustment defined by

$$\text{Roundness} \propto \frac{(\sigma_x - \sigma_y)}{\frac{(\sigma_x + \sigma_y)}{2}}, \quad (2)$$

where σ_x and σ_y are the standard deviations of the Gaussian fit in the x and y -axes, respectively. We tested several stars from the literature (e.g., [Cotten & Song 2016](#)) and, as a result, we concluded that those targets considered circular have the roundness smaller than 0.12, whereas non-circular objects have larger values. Applying this threshold to our sample, only 6 targets KIC 1868785, KIC 7267949, KIC 7435796, KIC 10533222, KIC 11092105 and KIC 11666436, survived all the image inspection criteria. The SEDs of the KIC 1868785, KIC 7267949, KIC 7435796, KIC 10533222, KIC 11092105 and KIC 11666436 stars, and their WISE images are shown in Figures 1 and 2, respectively.

3. RESULTS

Assuming that the detected IR excess in the stars KIC 1868785, KIC 7267949, KIC 7435796, KIC 10533222, KIC 11092105 and KIC 11666436 is related to IR radiation emitted by circumstellar dust, we modeled such excess using a simple blackbody function. A grid of blackbody temperatures ranging from 50 to 500 K at interval steps of 5 K (and 1 K, when necessary) was created, and performed the χ^2 minimization to choose the dust temperature T_d best fitting the observed excess, from where we obtained a temperature range of 265-484 K for the circumstellar dust.

In addition, we estimated three main dust properties, the fractional luminosity f_d , the dust radius R_d and the dust mass M_d . The fractional dust luminosity, defined as the ratio of the luminosity from the dust to that of the star, was estimated using the relationship between dust and stellar fluxes given by [Beichman et al. \(2005\)](#); considering that the detected excess for KIC 1868785, KIC 7267949, KIC 7435796, KIC 10533222, KIC 11092105 and KIC 11666436 has a peak emission at 12 μm wavelength, the minimum fractional luminosity was estimated, using values equals of 484 K, 293 K, 280 K, 341 K, 265 K and 336 K, for the dust temperature around each target, respectively, corresponding to the radiative temperature of a blackbody at 12 μm .

The disk radius or orbital R_d was computed considering the dusty material as optically thin and in thermal equilibrium with the stellar radiation field. With these considerations, and assuming that the dust grains behave similarly to a blackbody, a minimum distance for the circumstellar dust was estimated following the recipe by [Backman & Paresce \(1993\)](#). Finally, for the disk mass M_d estimation we have applied the recipe given by [Liu et al. \(2014\)](#). The computed debris disks physical parameters, temperature of the dust, radius of the debris disk, total mass of the disk of circumstellar material and the fractional luminosity of the dust are given in Table 1 together with stellar parameters.

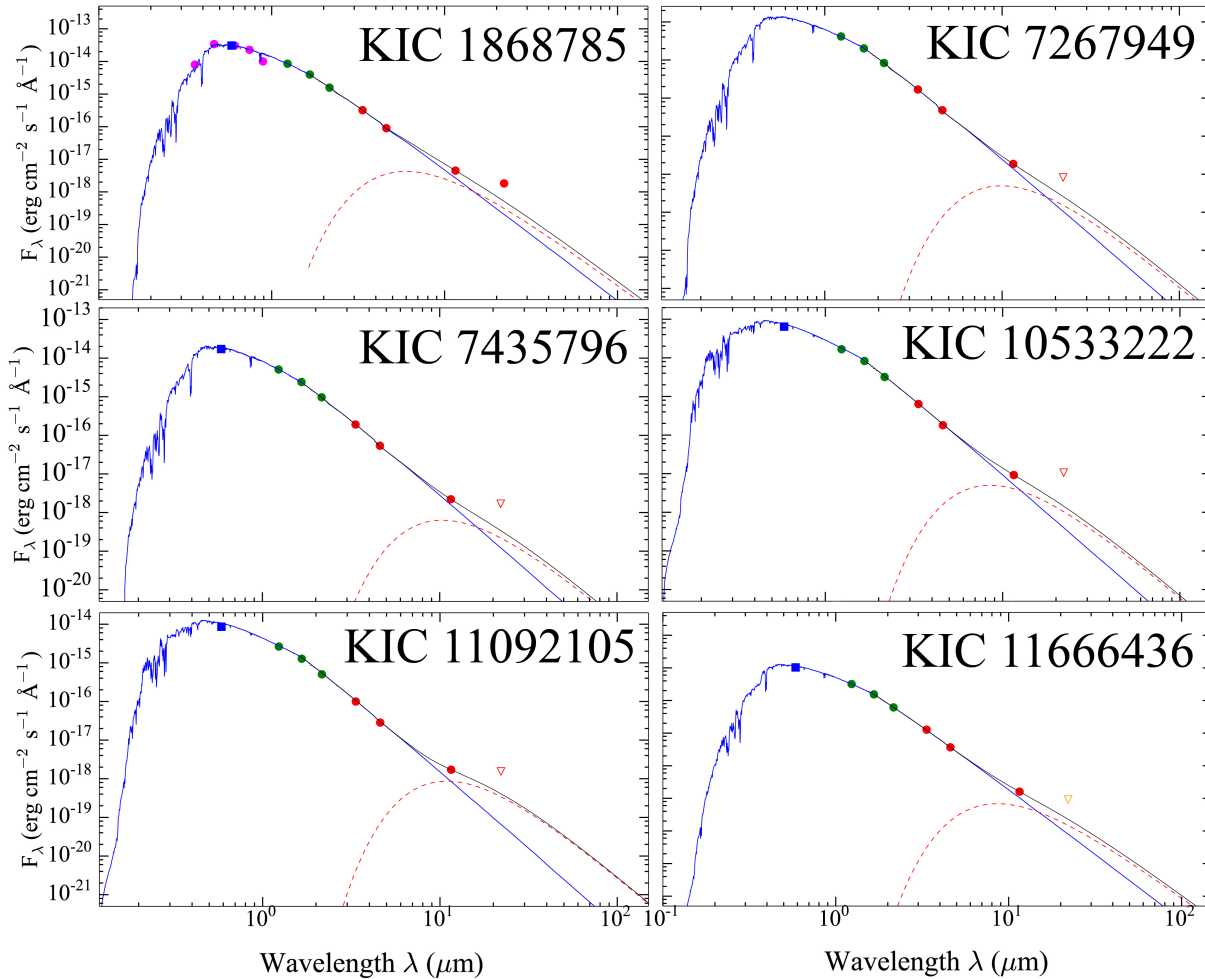


Figure 1. SEDs for stars with excess IR confirmed. The blue square represents the GAIA G-band flux (van Leeuwen et al. 2017). Magenta, red and green circles indicate the photometric data points from SDSS (ugriz filter) (Abazajian et al. 2009), 2MASS (JHK passbands) (Cutri et al. 2003), and WISE (Cutri et al. 2013), respectively. The blue solid line denotes the adjustment of the KURUCZ model (Castelli et al. 1997); the red dashed line means the best-fit using a simple blackbody model for WISE bands with IR excess and the black solid line is the sum of the two components.

4. CONCLUSIONS

This study reports the discovery of 6 *Kepler* main-sequence stars, typically solar rotational analogs with rotation period similar to the Sun’s values, presenting mid-IR excess compatible with the presence of debris disks. The dust temperatures obtained from the modeled IR excess range from 265 to 484 K, suggesting the presence of warm circumstellar material. The computed dust parameters

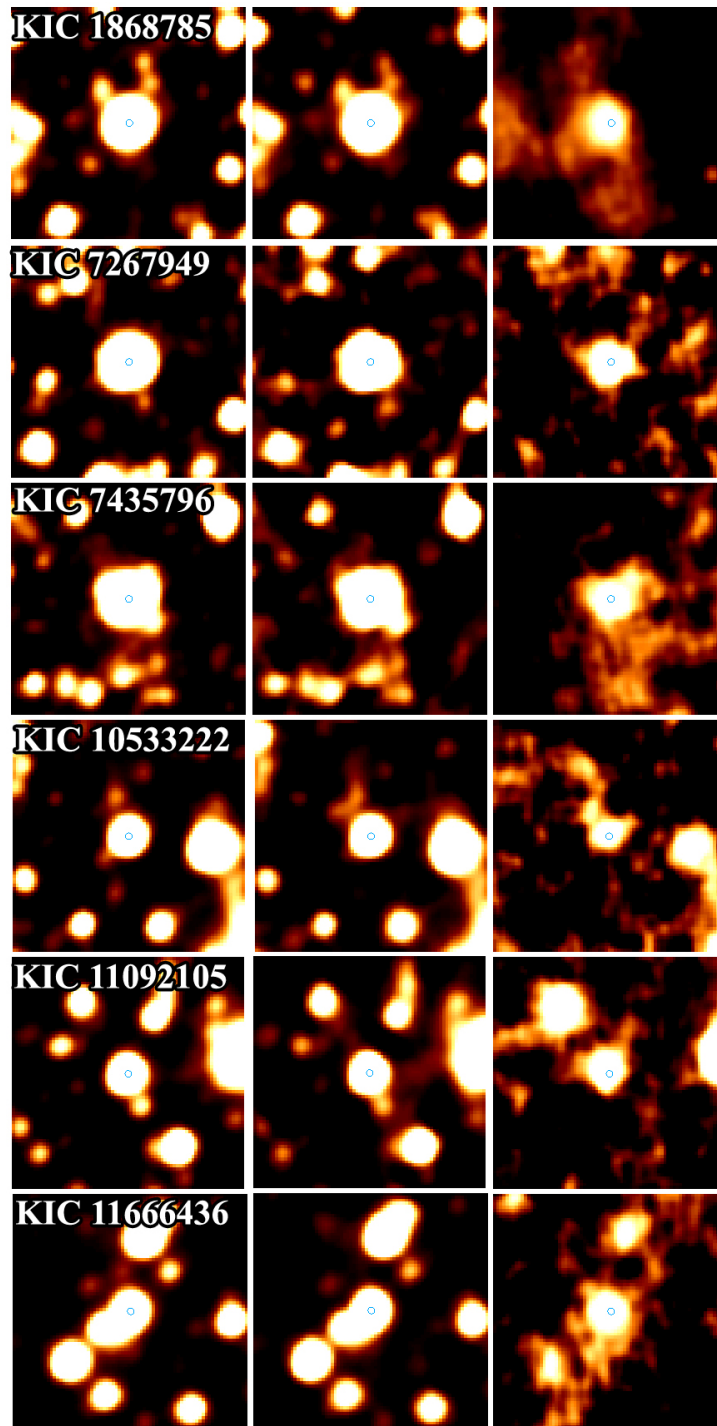


Figure 2. WISE images (from left to right: W1, W2, W3) for the six stars with IR excess confirmed in $12\ \mu\text{m}$, obtained from the Infrared Science Archive (IRSA) using $0\text{-}3\sigma$ linear scales around $1.7' \times 1.7'$. No contamination by artifacts has been found in the respective bands.

shows that the detected disks are located between 0.33 and 1.07 AU, at smaller orbital radii than the Solar System asteroid belt, that is from 2.0 and 3.5 AU (Wyatt 2008). Computed temperatures

indicate that the referred stars with IR excess present warm circumstellar dust with temperatures, in average, higher than the solar asteroid belt value. In effect, our finding may represent also an observational bias by considering that the presence of disks closer to the stars are hotter, and as a consequence, brighter if the IR excess is observed near the peak of their SEDs.

Circumstellar dust belts around main-sequence stars, as those reported in the present study, are composed of second-generation dust originated from the small-body population of planetary systems (Backman & Paresce 1993), which are mostly remnants of primordial protoplanetary disks (Hernández et al. 2007). These bodies can give fundamental informations about the chemistry and evolution of protoplanetary disk and the planetary systems they form. Despite a similar physical mechanism to be expected in the production of the reported debris disks, our findings show that stars with physical parameters similar to the Sun, as is the case of the whole sample here analyzed, can in fact be very different from the Sun once the star and its circumstellar environment are considered, confirming previous results by Da Costa et al. (2017). Among these physical parameters, age is an important one for determining the presence of debris disks. In the present work, based on gyrochronology estimations (e.g., Barnes et al. 2016; Ceillier et al. 2016), the stellar ages for our *Kepler* stars range around the solar age value, even though that range may be somewhat broad.

At the WISE wavelength bands, we are observing the Wien-edge of the energy distributions. In this sense, the lack of an excess for the large majority of the analyzed stars does not necessarily imply the absence of circumstellar material. Indeed, the detection of IR-excess, only in W3 band, is in agreement with Liu et al. (2014) assumption that the disk associated to this IR-excess are geometrically thin, that is, confined within a small radius range, with all the dust at the same temperature. The disks here reported may in fact be spatially extended and, by consequence, similar to the Solar System asteroid belt geometry. Their thin appearance may reflect the fact that only the inner edge of the disk can be detected with the present sensitivity. In addition, the absence

of detection in the W4 band may be explained by its considerably narrower range in comparison to W3. This fact would indicate that the fraction of solar rotational analog stars possessing debris disks could be higher than the fraction here observed. Nevertheless, the discovered debris disks are, by far, brighter and more massive than the Solar System zodiacal dust, a characteristic that allowed their detection. In this sense, the observation of solar debris disks at the distance of the refereed stars would be well below the WISE sensitivity level.

The present sample of debris disks has luminosity too high to be explained by a steady-state collisional cascade (Wyatt 2008; Gáspár et al. 2013) and a large amount of warm dust that cannot be sustained at the estimated stellar ages (Wyatt 2008). These unusual characteristics may reflect a possible disc-sculpting mechanism resulting from violent collisional events (e.g., Kral et al. 2015; Kenyon & Bromley 2005, 2006; Raymond et al. 2009; Zappalà et al. 2002; Durda et al. 2007).

Dust belts cooler than those reported here have their imprints at longer wavelength bands, and slight or no excess in the mid-IR. Therefore, the null detection of IR excess, at WISE sensitivity level, for the remaining 875 solar rotational analogue stars will certainly motivate new observational studies at far-IR, submillimeter and millimeter wavebands for a better characterization of material around these stars with a rotation period similar to that of the Sun. Furthermore, the presence of other disks structures (Wyatt 2008), in particular cold components like the *Kuiper* belt, and water ice traces, can be determined from observations in longer IR wavebands. In this sense, further observational studies are mandatory for the stars with detected IR excess here announced.

4.1. *Acknowledgments*

Research activity of the Observational Astronomy Board of the Federal University of Rio Grande do Norte (UFRN) is supported by continuous grants from CNPq and FAPERN Brazilian agencies. We also acknowledge financial support from INCT INEspaço/CNPq/MCT. A.D.C. acknowledges a

CAPES/PNPD fellowship. I.C.L acknowledges a CNPq/PDE fellowship. R.S.S., D.F.S., and M.N., acknowledge graduate fellowships from CAPES. This work is based on data products from the Wide-field Infrared Survey Explorer, a joint project of the University of California, Los Angeles, and the Jet Propulsion Laboratory/California Institute of Technology, supported by the National Aeronautics and Space Administration. This study has used NASA Astrophysics Data System (ADS) Abstract Service, the SIMBAD database, operated at CDS, Strasbourg, France, and data products from the Two Micron All-Sky Survey (2MASS), a joint project of the University of Massachusetts and the infrared Processing and Analysis Center, supported by the National Aeronautics and Space Administration and the National Science Foundation. This study has used VOSA support, developed under the Spanish Virtual Observatory project funded by the Spanish MICINN through grant AyA2011-24052. This study also includes data collected by the Kepler space mission. Funding for the Kepler mission is provided by the NASA Science Mission Directorate. We warmly thank the anonymous Reviewer for providing very helpful comments and suggestions.

REFERENCES

- Abazajian, K. N., Adelman-McCarthy, J. K., Agüeros, M. A., et al. 2009, *ApJS*, 182, 543
- Abe, Y., Ohtani, E., Okuchi, T., Righter, K., & Drake, M. 2000, in *Origin of the earth and moon*, eds. R. M. Canup, K. Righter, et al., 413
- Allard, F., Homeier, D., & Freytag, B. 2012, *RSPTA*, 370, 2765
- Aumann, H. H., Beichman, C. A., Gillett, F. C., et al. 1984, *ApJL*, 278, L23
- Backman, D. E., & Paresce, F. 1993, in *Protostars and Planets III*, ed. E. H. Levy & J. I. Lunine (Tucson: Univ. Arizona Press), 1253
- Barnes, S. A., Weingrill, J., Fritzewski, D., Strassmeier, K. G., & Platais, I. 2016, *ApJ*, 823, 16
- Bayo, A., Rodrigo, C., Barrado y Navascues, D., et al. 2008, *A&A*, 492, 277B.
- Beichman, C. A., et al. 2005, *ApJ*, 622, 1160
- Beichman, C. A., et al. 2006, *ApJ*, 652, 1674
- Castelli, F., Gratton, R. G., & Kurucz, R. L. 1997, *A&A*, 318, 841
- Ceillier, T., van Saders, J., García, R. A., et al. 2016, *MNRAS*, 456, 119
- Chen, C. H., et al. 2006, *ApJS*, 166, 351
- Cotten, T. H., & Song, I. 2016, *ApJS*, 25, 15
- Cutri, R. M., Skrutskie, M. F., van Dyk, S., et al. 2003, *VizieR Online Data Catalog: II/246*
- Cutri, R. M., Wright, E. L., Conrow, T., et al. 2013, *yCat*, 2328, 0
- Da Costa, A. D., Canto Martins, B. L., Leão, I. C., Lima Jr., J. E., Freire da Silva, D., de Freitas, D. B., De Medeiros, J. R., 2017, *ApJ*, 837, 15
- Das Chagas, M. L., Bravo, J. P., Costa, A. D., et al. 2016, *MNRAS*, 463, 1624
- DeMeo, F. E., & Carry, B. 2014, *Nature*, 505, 629
- Durda, D. D., Bottke, W. F., Nesvorný, D., et al. 2007, *Icarus*, 186, 498
- Gáspár, A., Rieke, G. H., & Balog, Z. 2013, *ApJ*, 768, 25
- Gray, D. F. 1992, *Camb. Astrophys. Ser.*, Vol. 20, 20
- Hernández, J., Hartmann, L., Megeath, T., et al. 2007, *ApJ*, 662, 1067
- Hsieh, H. H., & Jewitt, D. 2006, *Sci*, 312, 561
- Huber, D. et al. 2014, *ApJS*, 211, 2
- Jarrett, T., Cohen, M., Masci, F., et al. 2011, *ApJ*, 735, 112
- Kenyon, S. J., & Bromley, B. C. 2005, *AJ*, 130, 269
- Kenyon, S. J., & Bromley, B. C. 2006, *AJ*, 131, 1837
- Kral, Q., Thébault, P., Augereau, J.-C., Boccaletti, A., & Charnoz, S. 2015, *A&A*, 573, A39
- 158, 98
- Lanza, A. F. Rodonò, M., Pagano, I. et al. 2003, *A&A*, 403, 1135
- Liu, Q., Wang, T., & Jiang, P. 2014, *AJ*, 148, 3
- Maldonado, R. F., Chavez, M., Bertone, E., Cruz-Saenz de Miera, F. 2017, *MNRAS*, 471, 3419
- Martin, R. G., & Livio, M. 2012, *MNRAS*, 425, 6
- McQuillan A., Mazeh T., Aigrain S., 2014, *ApJS*, 211, 24 (McQ14)
- Mermilliod, J. C. 2006, *VizieR Online Data Catalog*, 2168, 0
- Moór A., Abrahm P., Derekas A., Kiss C., Kiss L. L., Apai D., Grady C., Henning T., 2006, *ApJ*, 644, 525
- Neckel, H. 1986 *A&A* 159, 175
- Patel, R. I., Metchev, S. A., & Heinze, A. 2014, *ApJS*, 212, 10
- Raymond, S. N., O'Brien, D. P., Morbidelli, A., & Kaib, N. A. 2009, *Icarus*, 203, 644
- Ribas, Á., Merín, B., Ardila, D. R., & Bouy, H. 2012, *A&A*, 541, A38
- Roberge, A., Chen, C. H., Millan-Gabet, R., et al. 2012, *PASP*, 124, 799
- Sibthorpe, B., Kennedy, G. M., Wyatt, M. C., et al. 2018, *MNRAS*, 475, 3046
- Sinclair, J. A., Helling, Ch., & Greaves, J. S. 2010, *MNRAS*, 409, L49
- Trilling D. E. et al., 2008, *ApJ*, 674, 1086
- van Leeuwen, F., Evans, D. W., De Angeli, F., et al. 2017, *A&A*, 599, A32
- Weissman, P. R. 1995, *ARA&A*, 33, 327
- Wyatt, M. C. 2008, *ARA&A*, 46, 339
- Wright E. L. et al., 2010, *AJ*, 140, 1868
- Zappalà, V., Cellino, A., dell'Oro, A., & Paolicchi, P. 2002, *Asteroids III*, 619

ONLINE DATA

Table 2. List of the 51 stars with IR excess for which $\chi_{12} \geq 2.0$ or $\chi_{22} \geq 2.0$ from three photospheric models: Kurucz-ATLAS9, BT-DUSTY, and BT-NextGen. The ellipsis (...) indicates upper limits for the WISE measurements.

KIC	RA	DE	Kurucz		NextGen		BT-Dust		excess?	
			χ_{12}	χ_{22}	χ_{12}	χ_{22}	χ_{12}	χ_{22}	W3	W4
1868785	291.57443	37.31554	6.08	3.20	5.75	3.18	5.75	3.18	Yes	Yes
3219127	286.57025	38.39762	2.16	...	2.01	...	2.01	...	Yes	No
3643036	290.73413	38.71746	3.22	2.92	3.11	2.91	3.11	2.91	Yes	No
4751492	293.19486	39.88782	2.20	...	2.11	...	2.11	...	Yes	No
4820062	286.56364	39.96158	2.20	No	No
4947417	297.54838	40.06008	6.21	...	6.18	...	6.18	...	Yes	No
5035733	297.72842	40.12920	9.60	8.77	9.53	8.77	9.53	8.77	Yes	Yes
5036092	297.79665	40.18130	4.21	...	4.03	...	4.03	...	Yes	No
5120654	297.01951	40.21359	9.93	4.87	9.71	4.86	9.71	4.86	Yes	Yes
5198141	294.87102	40.36343	2.27	...	2.12	...	2.12	...	Yes	No
5263998	288.34694	40.43668	...	2.05	...	2.06	...	2.06	No	Yes
5293988	296.67798	40.41841	6.09	...	6.01	...	6.01	...	Yes	No
5428470	284.34673	40.63319	2.37	...	2.19	...	2.19	...	Yes	No
5534914	292.24299	40.74677	...	2.41	...	2.41	...	2.41	No	Yes
5730371	298.05585	40.96706	11.19	7.04	11.10	7.03	11.10	7.03	Yes	Yes
5956717	290.62853	41.29013	2.09	...	2.15	...	2.15	...	Yes	No
6064473	297.64333	41.30418	4.62	5.83	4.62	5.83	4.62	5.83	Yes	Yes
6142317	296.86628	41.44202	...	2.12	...	2.12	...	2.12	No	Yes
6345900	284.64141	41.75273	2.06	No	No
6358701	290.02545	41.72927	2.49	...	2.43	...	2.43	...	Yes	No
6516101	289.85597	41.90501	4.83	2.01	4.70	2.01	4.70	2.01	Yes	Yes
6952979	293.17428	42.43163	3.50	...	2.83	...	2.83	...	Yes	No

Table 2. *Continued*

KIC	RA	DE	Kurukz		NextGen		BT-Dust		excess?	
			χ_{12}	χ_{22}	χ_{12}	χ_{22}	χ_{12}	χ_{22}	W3	W4
7267949	286.94895	42.82167	2.35	...	2.24	...	2.24	...	Yes	No
7435796	288.98419	43.03943	2.85	...	2.75	...	2.75	...	Yes	No
7457546	295.36482	43.03973	...	2.09	...	2.08	...	2.08	No	Yes
7763388	295.18879	43.42369	2.20	...	2.06	...	2.06	...	Yes	No
7772296	297.59851	43.44764	2.36	...	2.30	...	2.30	...	Yes	No
7953983	289.71354	43.72041	2.34	...	2.30	...	2.30	...	Yes	No
8042782	296.39621	43.85904	2.39	...	2.36	...	2.36	...	Yes	No
8328443	300.40546	44.26359	3.76	5.45	3.74	5.45	3.74	5.45	Yes	Yes
8429890	291.47401	44.48705	2.28	...	2.24	...	2.24	...	Yes	No
8441073	295.51828	44.44331	2.71	...	2.70	...	2.70	...	Yes	No
8565235	293.87219	44.64762	...	2.11	...	2.10	...	2.10	No	Yes
8718439	300.81718	44.82276	...	2.16	...	2.16	...	2.16	No	Yes
9161405	294.41346	45.55480	2.83	...	2.82	...	2.82	...	Yes	No
9410702	294.43354	45.91136	2.53	...	2.47	...	2.47	...	Yes	No
9896250	296.06648	46.72492	...	2.11	...	2.10	...	2.10	No	Yes
9946870	289.92768	46.85935	3.86	...	3.73	...	3.73	...	Yes	No
9963105	296.50230	46.87746	2.02	No	No
10468501	291.10030	47.66703	2.03	No	No
10533222	291.07269	47.71635	2.29	...	2.24	...	2.24	...	Yes	No
10613866	296.88037	47.81899	2.12	...	2.08	...	2.08	...	Yes	No
10670950	293.99346	47.95911	3.63	...	3.61	...	3.61	...	Yes	No

Fig. Set 3. SEDs and WISE images of the excluded stars from our sample.

Table 2. *Continued*

KIC	RA	DE	Kurukz		NextGen		BT-Dust		excess?	
			χ_{12}	χ_{22}	χ_{12}	χ_{22}	χ_{12}	χ_{22}	W3	W4
10972628	290.27466	48.48056	3.51	...	2.86	...	2.86	...	Yes	No
11074641	286.59790	48.63996	...	2.13	...	2.13	...	2.13	No	Yes
11092105	295.56162	48.64493	4.05	...	4.02	...	4.02	...	Yes	No
11135275	290.67574	48.72052	...	2.19	...	2.19	...	2.19	No	Yes
11177716	284.26121	48.88640	2.47	...	2.37	...	2.37	...	Yes	No
11352643	293.02650	49.18330	3.40	...	3.31	...	3.31	...	Yes	No
11666436	294.26457	49.73296	2.64	...	2.29	...	2.29	...	Yes	No
12256697	290.46572	50.93251	2.98	2.20	2.80	2.19	2.80	2.19	Yes	Yes

Table 3. Visual inspection of WISE images for a sample of 47 stars with IR exces.

KIC	visual inspection	Disk
1868785	Isolated single source in W3	Yes
3219127	Non-circular sources in W3	No
3643036	Offset source in W3 and W4	No
4751492	Absent source in W3	No
4947417	Absent source in W3	No
5035733	Absent source in W3 and W4	No
5036092	Offset source in W3	No
5120654	Absent source in W3 and W4	No
5198141	Confusion of sources in W3	No
5263998	Offset source in W4	No
5293988	Offset source in W3	No
5428470	Non-circular source in W3	No
5534914	Offset source in W4	No
5730371	Absent source in W3 and W4	No
5956717	Offset source in W3	No
6064473	Absent source in W3 and W4	No
6142317	Offset source in W4	No
6358701	Offset source in W3	No
6516101	Non-circular source in W3 and absent source in W4	No
6952979	Confusion of sources in W3	No
7267949	Isolated single source in W3	Yes
7435796	Isolated single source in W3	Yes
7457546	Absent source in W4	No
7763388	Non-circular source in W3	No

Table 3. *Continued*

KIC	visual inspection	Disk
7772296	Absent source in W3	No
7953983	Offset source in W3	No
8042782	Offset source in W3	No
8328443	Absent source in W3 and W4	No
8429890	Absent source in W3	No
8441073	Absent source in W3	No
8565235	Absent source in W4	No
8718439	Absent source in W4	No
9161405	Absent source in W3	No
9410702	Non-circular source in W3	No
9896250	Absent source in W4	No
9946870	Non-circular source in W3	No
10533222	Isolated single source in W3	Yes
10613866	Offset source in W3	No
10670950	Confusion of sources in W3	No
10972628	Offset source in W3	No
11074641	Absent source in W4	No
11092105	Isolated single source in W3	Yes
11135275	Offset source in W4	No
11177716	Absent source in W3	No
11352643	Non-circular source in W3	No
11666436	Isolated single source in W3	Yes
12256697	Non-circular source in W3 and absent in W4	No

Table 4. Stellar parameters for the stars with confirmed IR excess. Effective temperature (T_*), surface gravity ($\log g$), metallicity ($[Fe/H]$), radius (R_*) and mass (M_*) were obtained from [Huber et al. \(2014\)](#), whereas luminosity (L_*) was computed using these parameters. Rotation periods (P_{rot}) were taken from [McQuillan et al. \(2014\)](#).

KIC	T_* (K)	$\log g$	[Fe/H]	R_* (R_\odot)	M_* (M_\odot)	L_* (L_\odot)	P_{rot} (days)
1868785	5837±166	4.50±0.29	-0.16±0.32	0.974±0.079	1.083±0.141	0.988±0.275	24.219±0.232
7267949	5629±159	4.42±0.13	-0.42±0.36	0.900±0.131	0.775±0.049	0.729±0.373	25.109±0.457
7435796	5902±170	4.43±0.06	0.14±0.18	1.045±0.107	1.072±0.129	1.188±0.342	29.217±0.362
10533222	5926±176	4.29±0.16	-0.12±0.26	1.176±0.209	0.976±0.107	1.530±0.537	24.338±0.528
11092105	5658±162	4.52±0.04	-0.20±0.28	0.852±0.076	0.885±0.079	0.667±0.255	25.808±0.429
11666436	5604±155	4.56±0.03	-0.20±0.30	0.815±0.064	0.887±0.088	0.587±0.222	23.923±0.579

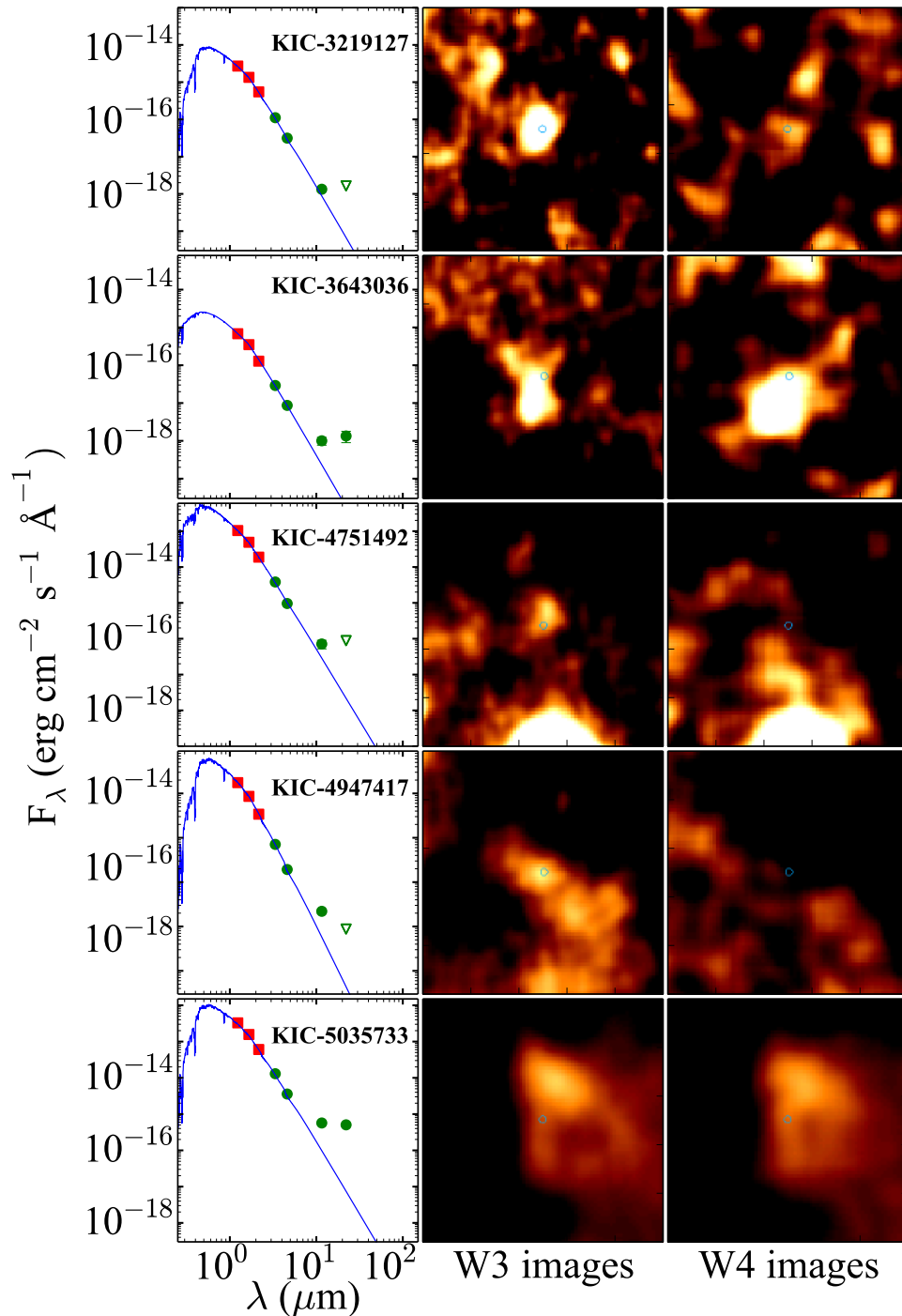


Figure 3. SEDs and WISE images of KIC 3219127, KIC 3643036, KIC 4751492, KIC 4947417, and KIC 5035733 stars with apparent IR excesses, but presenting fundamental problems in the images. *Left panels:* SED of each individual target. Red squares represent the fluxes from the 2MASS JHK passbands (Cutri et al. 2003). Green circles display the fluxes from WISE W1-W4 bands (Cutri et al. 2013). The WISE upper limits are indicated by green open triangles. The blue solid line denotes the adjustment of the Kurucz model (Castelli et al. 1997). *Center/Right panels:* respective stellar WISE W3/W4 images. The complete figure set (with 9 subsets comprising 41 targets) is available in the online journal.